Available online at www.sciencedirect.com
SCIENCE DIRECT®
Carbohydrate Research 340 (2005) 1051–1057
Carbohydrate RESEARCH

Potential transition-state analogs for glycosyltransferases. Design and DFT calculations of conformational behavior☆

Michal Raab, Stanislav Kozmon and Igor Tvaroška*

Institute of Chemistry, Slovak Academy of Sciences, Dúbravska cesta 9, 845 38 Bratislava, Slovakia

Received 7 October 2004; accepted 18 January 2005

Dedicated to Professor David A. Brant

Abstract—The structure of a previously calculated transition state (TS) was used to design the [tetrahydro-2-(methylthio)furan-2-yl]methyl phosphate dianion (**1**) as a new scaffold for transition-state analogs of reactions catalyzed by the inverting glycosyltransferases. This scaffold contains relevant features of the donor and acceptor and represents a new type of potential inhibitors for these enzymes. Available conformational space of **1** was explored using DFT quantum chemical methods by means of two-dimensional potential-energy maps calculated as a function of Φ, Ψ, and ω dihedral angles at the B3LYP/6-31+G* level. The calculated potential energy surfaces revealed the existence of several low-energy domains. Structures from these regions were refined at the 6-311++G** level and led to 14 conformers. The stability of conformers is influenced by their environment, and in aqueous solution two conformers dominate the equilibrium. A superposition of calculated conformers with the predicted TS structure revealed that the preferred conformers in solution nicely mimic structural features of the TS. These results imply that **1** has structural properties required to mimic the TS and therefore can be used as a scaffold for further development of TS-analog inhibitors for retaining glycosyltransferases.

Keywords: Glycosyltransferases; Transition-state analog; Inhibitors; Conformation; Density functional; Ab initio calculations

1. Introduction

Glycosyltransferases encompass a group of enzymes that are involved in the biosynthesis of *N*- and *O*-linked glycan parts of glycoproteins.[1–4] Many functions have been implicated for protein glycosylation, including promoting protein folding in the ER,[5] stabilizing cell-surface glycoproteins,[6] and providing recognition epitopes that activate the innate immune systems.[7] It is therefore not surprising that genetic mutations that modify the activity of glycosyltransferases can lead to serious physiological disorders and can be lethal in animals as well as in humans.[8] Changes in protein glycosylation are early indicators of cellular changes in many diseases. Therefore, in selected cases, glycosyltransferases are validated targets for therapeutic intervention. Consequently, the development of potent and specific inhibitors for glycosyltransferases has attracted increasing interest.[9,10]

Different strategies have been used in order to identify potent inhibitors of glycosyltransferases.[9–16] Despite an increasing number of potential inhibitors, only a few of them have exhibited significant activity. Though transition-state (TS) analogs have enormous potential and are valued tools for drug discovery as potent and specific inhibitors of enzymes, to date, the ability to generate transition-state analogs of glycosyltransferases has largely remained elusive. The underlying concept for TS-analog inhibitors[17–19] has its roots in the specific stabilization of the transition state by interactions in the catalytic site of the enzyme. It can be shown that perfect TS analogs should bind more tightly to the enzyme than the reactants by huge factors, ranging up to 10-fold[17] in some cases.[18] Recent ab initio studies of the catalytic

☆ This paper is in honor of the great contributions to carbohydrate chemistry that have been made by Professor David A. Brant.

* Corresponding author. Tel.: +421 2 5477 2080; fax: +421 2 5941 0222; e-mail: chemitsa@savba.sk

0008-6215/$ - see front matter © 2005 Elsevier Ltd. All rights reserved.
doi:10.1016/j.carres.2005.01.041

mechanism of inverting glycosyltransferases[20,21] provided an opportunity to design a new generation of inhibitors, based on a scaffold that imitates the transition state of the enzymatic reaction rather than the ground state, promising better inhibition than the natural carbohydrate substrate. In this paper we design a new scaffold that represents a potential TS analog. Then we explore conformational space available for this structure using density functional theory (DFT) calculations and determine the structure of conformers to provide necessary information to assess structural similarity between a scaffold and the TS.

2. Results and discussion

2.1. Design of a TS analog

A transition-state analog is a stable compound that structurally resembles the three-dimensional structure and charge distribution of a substrate(s) portion of the unstable TS of an enzymatic reaction. Rational design of glycosyltransferase inhibitors still remains a difficult task due to intrinsic features of glycosyltransferases: a complex of a four-partner transition state (donor and acceptor sugar, metal, and nucleotide), weak binding of the enzyme with their natural substrates (usual K_m values are in the millimolar range), and few structural data. It is obvious that design of transition-state analog inhibitors of an enzyme requires knowledge of the mechanism of the enzymatic reaction and the structure of the TS. In our previous studies we have investigated the catalytic mechanism and main structural features of the TS were determined for inverting glycosyltransferases,[20] and later the structure of the transition state (Fig. 1) for the UDP-*N*-acetylglucosamine: α-1,3-D-mannoside β-1,2-*N*-acetylglucosaminyltransferase I (*N*-acetylglucosaminyltransferase I, GnT-I, EC 2.4.1.101) was refined[21] using the structural information available for this enzyme.[22] These ab initio calculations[20,21] revealed the following main characteristics of the transition state: (a) the hexopyranose ring conformation resembles a half-chair conformation with the oxocarbenium character at the anomeric carbon; (b) the C-1–O-1 distance is a considerably longer (2.3–2.7 Å); (c) a new β-glycosidic bond is being created with the bond length larger (1.9 Å) than the normal bond length; the forming and breaking bonds are oriented almost perpendicularly with respect to the plane defined by C-2–C-1–O-5 atoms of the pyranose ring. It is clearly evident that the transition state for a glycosyltransferase consists of the deformed nucleotide sugar and acceptor oligosaccharide, linked in a specific mutual arrangement. It would not be possible to design a stable molecule, that mimics the transition state closely, because of the foregoing described characteristics of the TS. However, even crude TS analogs incorporating all relevant features

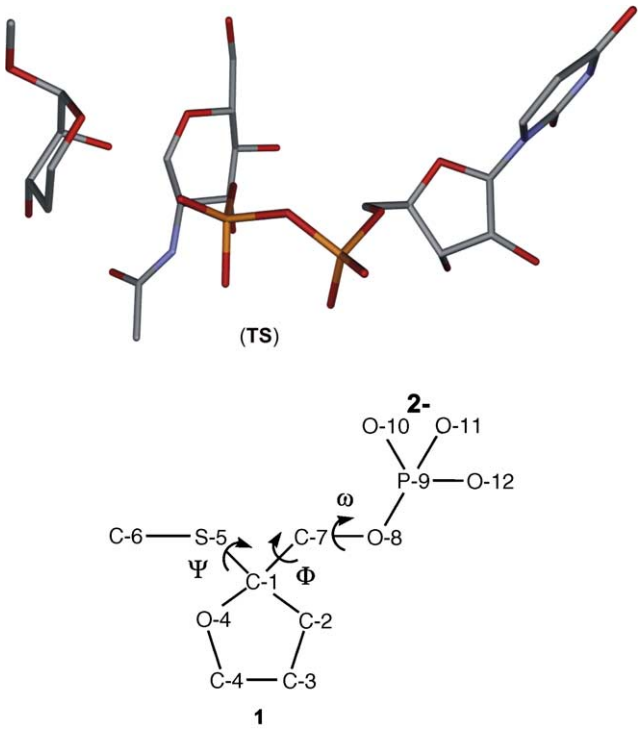

Figure 1. Schematic representation of the predicted TS structure[21] (**TS**) and the [tetrahydro-2-(methylthio)furan-2-yl]methyl phosphate dianion (**1**).

would be expected to be excellent reversible inhibitors. To achieve this, the TS analog should contain the main structural features of the TS from the acceptor and donor. The calculated structure[21] of a TS model for GnT-I provided a blueprint for the design of a new scaffold that might mimic the TS. In this case, we focused on functional groups linked to the center of the catalytic reaction, which is the anomeric carbon of the donor. The main concern was to design a scaffold that would properly mimic distances between the anomeric carbon (C-1) and both the leaving group and the acceptor. The proposed structural mimic is the [tetrahydro-2-(methylthio)furan-2-yl]methyl phosphate dianion (**1**) shown in Figure 1. The structural features of the TS are represented in **1** as follows: the enlarged C-1–O-1 distance presented in the TS is accomplished by linking a methyl phosphate group to C-1. In this moiety, the C-1–O-8 distance between the anomeric carbon and the phosphate oxygen is 2.4 Å, which is very close to the corresponding distance in the TS; the length of the C-1–S-5 bond is 1.9 Å, similar to the distance between the anomeric carbon and the attacking oxygen in the TS; and the C-1–C-6 distance of 2.9 Å corresponds to the distance in the TS. A deformed monosaccharide ring in the TS is represented by a five-membered ring, for the sake of simplicity, without substituents. The most difficult part of the TS to mimic appeared to be the almost linear arrangement of substituents (the leaving and attacking oxygen atoms) at the anomeric center (O–C–O angle); in the case

of **1**, the corresponding bond angle C-7–C-1–S-5 is smaller, and is close to 110°. Next we describe the structure and conformational behavior of **1**, and compare the resulting conformers with the structure of the TS, which is prerequisite for any further rational design of inhibitors.

2.2. Conformational analysis of 1

Although the literature reports some modeling studies on conformational properties of carbohydrate–phosphate linkages,[23–25] we are not aware of any modeling study on the structural moiety occurring in the [tetrahydro-2-(methylthio)furan-2-yl]methyl phosphate dianion. The orientation around the anomeric linkages and conformation of the methyl phosphate group in **1** is described by three internal rotational degrees of freedom associated with the C-1–C-7, C-1–S-5, and C-7–O-8 bonds (Fig. 1). The balance of electrostatic, steric, and lone-pair interactions governing the conformation of each individual group, methyl phosphate or methylthio, is further complicated by the linkage of both groups to the same carbon atom. Therefore, the available conformational space was monitored by means of a series of two-dimensional (Φ, Ψ) potential-energy surfaces (PES), each one corresponding to the one from three different starting values of ω, namely $\omega = 60°$ (*G*), $\omega = -60°$ (*mG*), and $\omega = 180°$ (*T*). Although we did not fully explore whole conformational space, especially in the ω-direction, this procedure supplies a representative number of conformers. Figure 2 represents the B3LYP/6-31+G* conformational-energy maps of the *G*, *mG*, and *T* rotamers around the C-7–C-8 bond (ω torsion angle) for **1** calculated as a function of the torsion angles Φ and Ψ. Several energy minimum domains (M1–M14) were found on each of these maps. In the case of the *G* ($\omega \sim 60°$) rotamer (Fig. 2a), three distinct low-energy regions having (Φ, Ψ) values close to (30°, 270°), (180°, 180°), and (180°, 270°), respectively, were identified; on the map for the *mG* ($\omega \sim -60°$) rotamer (Fig. 2b), five regions were found (60°, 300°), (180°, 270°), (240°, 210°), (300°, 60°), and (300°, 300°), respectively; and in the case of the *T* ($\omega \sim 180°$) rotamer (Fig. 2c), six regions can be seen, namely (60°, 270°), (180°, 180°), (180°, 270°), (270°, 60°), (270°, 180°), and (300°, 270°), respectively. The maps clearly show how interactions between the two groups linked to the anomeric carbon influence the available conformational space for **1**. For example, all three (Φ, Ψ) maps lack a low-energy region in the (60°, 60°) area, although for the individual C–S or C–C bond the +*gauche* conformation corresponds to a local minimum.[26] Geometries from all these regions were used as the initial geometry for further optimizations of **1**, allowing also the torsion angles Φ, Ψ, and ω to relax. The optimization at the B3LYP/6-311++G** level led to 14 distinct minima, which is a much lower number than 27 minima based on an assumption of three staggered conformation for each bond.

The values of Φ, Ψ, and ω dihedral angles and others selected angles [$\tau_1 = \tau$(C-4–O-4–C-1–S-5), $\tau_2 = \tau$(C-4–O-4–C-1–C-7), $\tau_3 = \tau$(C-4–O-4–C-1–C-2), and $\alpha = \alpha$(S-5–C-1–C-7)] of 14 resulting conformers (M1–M14) are given in Table 1. The relative energies of the 14 minima calculated for **1** in gas phase and aqueous solution are reported in Table 2, together with the estimated percentage contribution of each conformer of **1** to the equilibrium at 298 K. From values presented in Table 2 it is clear that conformational preference around the C-1–X bonds in **1** is strongly influenced by solvent. Vacuum calculations predict eight conformers in equilibrium M2:M9:M5:M14:M12:M6:M10:M11 = 62:16:12:3:3:2:1:1 with the M2 as the preferred conformer. The M2 conformer exhibits the *trans* orientation around the both anomeric linkages. On the other hand, in aqueous solution, the equilibrium of conformers is considerably shifted as compared to the gas phase. The stability of M8 and M9 conformers is enhanced by solvent and these conformers are close in their free energies and dominate the equilibrium mixture with M8:M9 = 55:44. The ab initio potential energy profile for rotation around the anomeric C-1–X linkages in the six-membered ring, which is influenced by the *exo*-anomeric effect,[27] have been previously investigated in detail[26] and preference for the *gauche* over *trans* conformation has been observed for the C-1–X bond in *C*- and *S*-glycosyl compounds. The predicted preference for the orientation around C–X anomeric bonds linked to the five-membered ring in **1** is different. As may be seen from Tables 1 and 2, calculations predicted that only two of three staggered orientations around the C-1–S-5 bond are populated, namely *mG* and *T*; the *G* orientation is not populated as the M7 and M13 conformers possessing this arrangement of the Ψ dihedral angle have too high a relative free energy. For the orientation around the C-1–C-7 bond in the gas phase, the *T* and *mG* orientations are preferred, although the *G* orientation is also to some extent present. In aqueous solution the *mG* orientation around the C–C anomeric bond is dominant. The structural features of the relevant conformers are illustrated in Figure 3, which shows the structures of the M2, M5, M8, and M9 conformers.

The foregoing discussion concerned only the conformation of the two substituents at the anomeric carbon. However, the potential TS analog **1** has flexibility of the furanose ring as the other degree of conformational freedom. It is well known that the five-membered furanose ring is more flexible as compared to six-membered pyranose ring and can adopt several ring conformations. Therefore, we did not explore all possible ring shapes during our conformational analysis. Instead, for each calculated PES point, the ring geometrical variables were fully optimized without constraints. Moreover, it

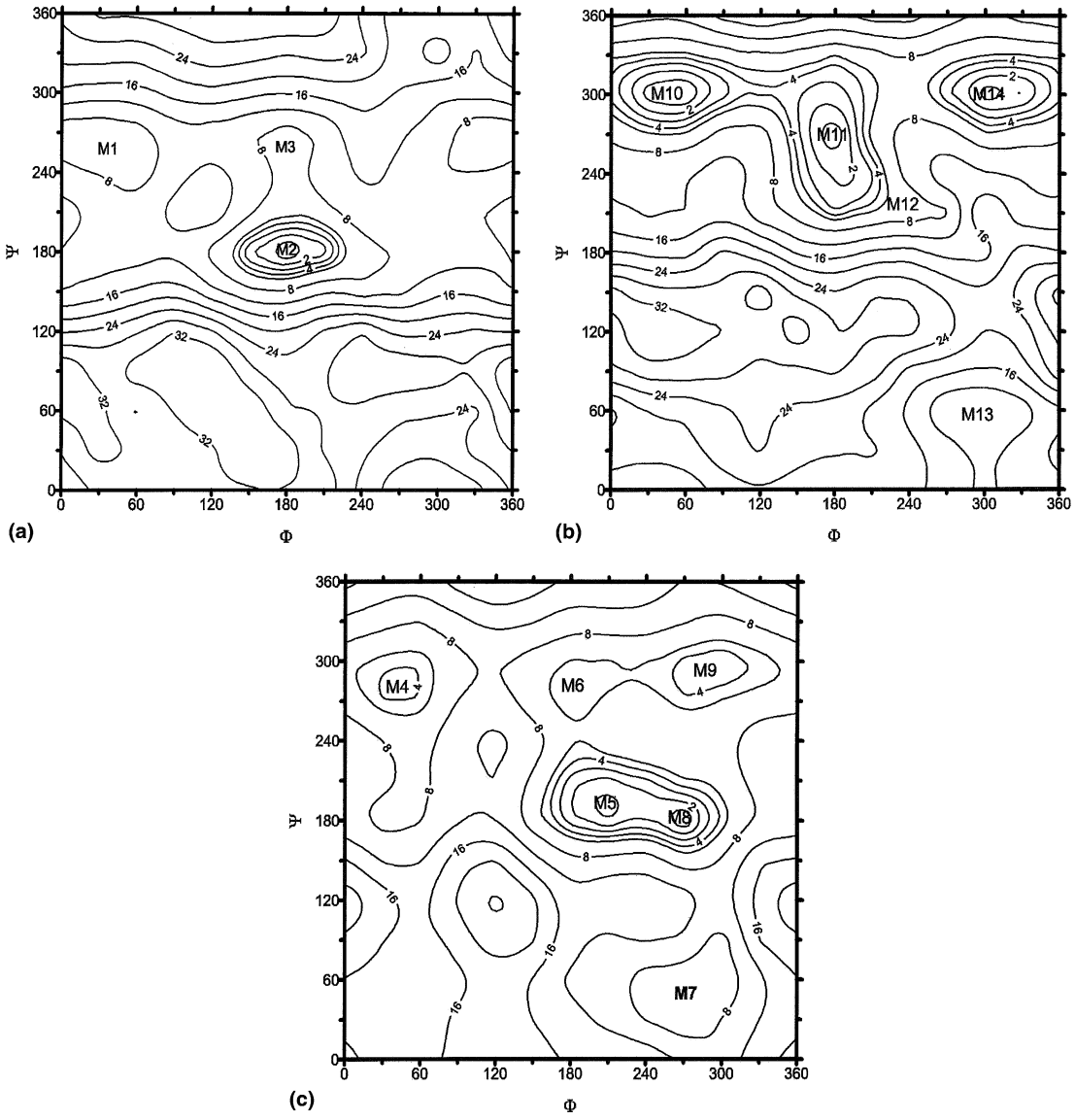

Figure 2. Relaxed conformational energy maps of [tetrahydro-2-(methylthio)furan-2-yl]methyl phosphate dianion (**1**) calculated at the B3LYP/6-31+G* level as a function of the torsional angles Φ and Ψ, with the torsional angle ω in *G* (a), *mG* (b), and *T* (c) orientation. The symbols M indicate local minima.

is well documented that the shape of the five-membered ring depends on the character and the orientation of the ring substituents. A similar behavior has been found in the case of **1**. The calculated results clearly show (Table 1) that ring conformation depends on orientation of substituents at the anomeric carbon, and several different conformations were predicted. The E_3 conformation is the preferred shape of the furanose ring in **1** and occurs in five conformers. Interestingly, the E_3 conformation was predicted for all dominant conformers, except for one. The characteristic feature of the E_3 conformation is that atoms C-4, O-4, C-1, and C-2 are nearly coplanar, which is documented by the dihedral angle $\tau_3 = \tau$(C-4–O-4–C-1–C-2) shown in Table 1 and resembles the arrangement at the anomeric carbon in the calculated structure of the TS for inverting glycosyltransferases.[20,21]

A structural similarity between the transition-state and its analog is a key factor determining the binding properties of TS analogs. The DFT conformational analysis of the potential TS analog **1** provided a set of conformers that can be used to assess how this new scaffold mimics the calculated TS structure for glycosyltransferases. Generally, most of the conformers nicely overlap with the corresponding part of the TS structure. It appears that the best superposition was found for the M9 conformer. This superposition is shown in Figure 4. It may be seen that structural parts of the M9 conformer closely overlap with the corresponding parts of the TS; the furanose ring oxygen with

Table 1. DFT/ab initio calculated geometrical parameters of the [tetrahydro-2-(methylthio)furan-2-yl]methyl phosphate dianion (**1**) conformers at the B3LYP/6-311++G** level[a]

Name	Φ	Ψ	ω	τ_1	τ_2	τ_3	α	Ring
M1	50.1	−108.7	93.5	108.5	−137.9	−17.1	104.2	E_4
M2	179.6	176.2	85.8	101.0	−139.6	−21.6	112.4	^2E
M3	179.9	−113.7	92.8	115.2	−127.3	−11.0	110.7	^3E
M4	49.2	−62.0	−107.9	89.6	−154.1	32.8	106.7	E_1
M5	171.7	176.6	113.7	130.7	−110.5	8.7	111.9	E_3
M6	169.6	−82.9	−100.1	86.2	−156.0	−37.5	109.2	E_1
M7	−90.0	47.2	153.6	73.4	−159.2	−44.3	114.1	^0E
M8	−86.0	−174.9	−151.5	129.0	−106.2	9.5	114.2	E_3
M9	−57.1	−64.8	−115.8	123.3	−114.6	1.3	112.0	E_3
M10	54.3	−53.5	−93.9	94.3	−150.2	−29.2	106.1	E_4
M11	176.5	−89.7	−91.5	133.5	−109.7	7.5	109.2	^3E
M12	172.5	−89.5	−107.3	117.9	−124.3	−5.7	109.6	E_3
M13	−66.0	46.4	−131.2	71.3	−162.5	−46.4	113.4	^0E
M14	−53.4	−60.3	−103.4	120.9	−117.8	−2.0	111.1	E_3

[a] Angles in degrees.

Table 2. DFT/ab initio calculated relative energies (ΔE, kcal/mol), zero point energy (ZPE), entropy[a] (ΔS, cal/mol deg), thermal energy corrections (ΔH_{298}), solvation energy (ΔE_{solv}), free energy in vacuum and aqueous solution (ΔG_{gas}, ΔG_w) and estimated equilibrium percentages (x, %) of the [tetrahydro-2-(methylthio)furan-2-yl]methyl phosphate dianion (**1**) conformer

Conformer	ΔE	ZPE	ΔS	ΔH_{298}	ΔG_{gas}	x_{gas}	E_{solv}	ΔG_w	x_w
M1	4.47	111.98	113.09	8.58	5.11	0.0	−224.13	7.07	0.0
M2	0.00	112.42	117.92	8.95	0.00	62.1	−229.52	8.03	0.0
M3	5.07	112.08	114.88	8.59	5.29	0.0	−224.36	7.24	0.0
M4	1.83	112.18	113.56	8.62	2.58	0.8	−227.35	5.94	0.0
M5	0.47	112.06	113.70	8.55	0.98	11.9	−230.21	3.63	0.1
M6	0.92	112.61	113.14	8.47	2.06	1.9	−225.83	9.86	0.0
M7	7.56	112.47	117.56	8.96	7.74	0.0	−237.14	3.21	0.2
M8	3.58	112.20	110.55	8.36	4.97	0.0	−236.70	0.00	55.0
M9	1.57	112.06	119.98	9.17	0.82	15.5	−232.86	0.13	44.2
M10	2.19	112.19	115.12	8.62	2.47	1.0	−231.08	6.03	0.0
M11	0.74	112.43	110.32	8.38	2.46	1.0	−232.93	7.27	0.0
M12	0.11	112.47	110.24	8.34	1.85	2.7	−230.20	8.18	0.0
M13	6.71	112.32	114.52	8.58	7.26	0.0	−228.80	6.50	0.0
M14	1.43	111.99	114.33	8.64	1.77	3.1	−228.61	2.86	0.4

[a] Angles in degrees.

the pyranose ring oxygen, sulfur with the attacking oxygen, methyl carbon with the acceptor carbon atom, and phosphate oxygen from M9 with the phosphate oxygen of the leaving group of donor. Our calculations clearly show that the suggested scaffold for potential transition-state analogs can adopt conformations that have very similar structural features as those predicted for the TS of reaction catalyzed by inverting glycosyltransferases. It is obvious that this scaffold is only a basis for further refinement, which might involve various modifications of substituents on the furanose ring to mimic a transferred monosaccharide, and a substitution of methyl group linked to sulfur atom by various larger substituents mimicking the acceptor monosaccharide. The latter variations might be especially crucial for the potency and specificity of design inhibitors, since it is well known that there is a limited number of donor nucleotides and a very large number of possible acceptors that most likely define the specificity of glycosyltransferases. This superposition also revealed that the phosphate dianion in **1** is properly oriented to interact with a bivalent metal cofactor presented in the active site of inverting glycosyltransferases. Although this kind of electrostatic interactions is very strong, it remains to be seen whether these interactions are sufficient to mimic the UDP (uridine 5′-diphosphate) part of the donor. Compounds based on the scaffold suggested and explored in this study are being synthesized in laboratories of our Institute, and their activity is to be tested against several glycosyltransferases.

In conclusion, we have suggested a new scaffold for transition-state analogs of reactions catalyzed by the inverting glycosyltransferases. The conformational properties of the [tetrahydro-2-(methylthio)furan-2-yl]-methyl phosphate dianion (**1**) were explored using DFT/ab initio method and the stability of the calculated conformers was estimated for the gas phase and for aqueous solution. It was predicted that while eight conformers are in equilibrium in the gas phase, just two conformers (M8 and M9) dominate the equilibrium in aqueous solution. The resulting structures were compared with the structure of the TS previously predicted.

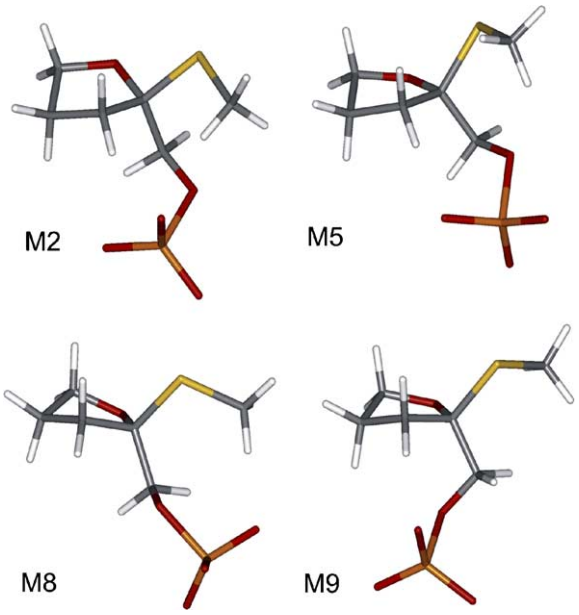

Figure 3. Comparison of the three-dimensional structure of the preferred conformers of the [tetrahydro-2-(methylthio)furan-2-yl]methyl phosphate dianion (**1**) calculated at the B3LYP/6-311++G** level.

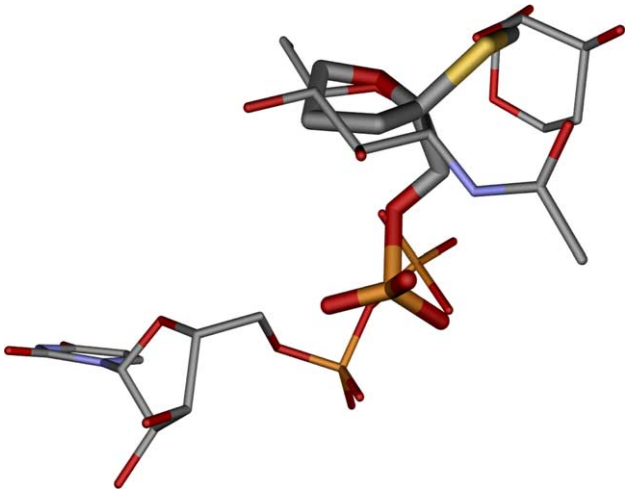

Figure 4. Superposition of the predicted transition-state (**TS**) structure[21] and the M9 conformer of the [tetrahydro-2-(methylthio)furan-2-yl]methyl phosphate dianion (**1**).

A clear similarity between the proposed scaffold **1** and the TS structures is observed, which implies that **1** might have the properties of a transition-state analog.

3. Experimental

3.1. Computational procedures

The linkages of the methyl phosphate and methylthio groups to the anomeric carbon atom of the furan ring result in three internal rotational degrees of freedom associated with the orientation of these groups. For **1** the rotation around the 'anomeric linkage' C–S is described by dihedral angle $\Psi = \Psi$[O-4–C-1–S-5–C-6] and the orientation of the methyl phosphate group by dihedral angles $\Phi = \Phi$[O-4–C-1–C-7–O-8] and $\omega = \omega$[C-1–C-7–O-8–P-9], respectively. Conformational analysis was focused on the influence of the methyl phosphate and methylthio group orientations on the total energy, as a function of three torsion angles. To get a concise picture of the conformational preference, the available conformational space was monitored by means of a series of two-dimensional (Φ, Ψ) potential-energy surfaces (PES), each one corresponding to that from three different starting values of ω, namely $\omega = 60°$, $\omega = -60°$, and $\omega = 180°$. These ω values characterize the +*gauche* (*G*), −*gauche* (*mG*), and *trans* (*T*) rotamer around the C–O linkage, respectively. Torsional angles Φ and Ψ were varied by 30° increments within the 0–360° range. During the optimization, all geometrical parameters except the dihedral angles Φ, Ψ, and ω were optimized. As a result, each calculated point of the three PES's corresponds to the most stable geometrical conformation of the structure for the fixed values of Φ, Ψ, and ω. The location of the local minima is only approximate; therefore a further optimization without constraints of fixed dihedral angles was required. The calculations were carried out using the Jaguar program[28] on QS8-2800C.[29] The optimization of the geometry was performed using the B3LYP density functional method[30] with the 6-31+G* basis set. The geometries of all local minima identified on the maps were then fully optimized with no constraints on the Φ, Ψ, and ω torsion angles the B3LYP/6-311++G** basis set. For all minima of **1**, the vibrational frequencies were calculated at the B3LYP/6-31+G* level, and zero-point energy, thermal and entropy corrections were evaluated using standard statistical thermodynamics methods based on the ideal-gas rigid-rotor model.[31] Finally, the solvent effects on the conformational equilibrium were investigated with a self-consistent reaction field method[32] as implemented in the Jaguar program[28] at the level B3LYP/6-31+G*, using the Poisson–Boltzmann solver and including empirical corrections to repair deficiencies in both ab initio and continuum solvation models. Solvation calculations were carried out for water ($\varepsilon = 80.37$). This approach correctly predicts the pK_a values for a large set of different molecules,[28] and we expect the solvation energies to be reasonable well predicted. Then the percentage contribution of each conformer of **1** to the conformational equilibrium at 298 K was determined through the Boltzmann equation.

Acknowledgements

This work was supported by the grants from Mizutani Foundation for Glycoscience No. 040013 and from

Science and Technology Assistance Agency under No. APVT-51-044902.

References

1. Beyer, T. A.; Sadler, J. E.; Rearick, J. I.; Paulson, J. C.; Hill, R. L. *Adv. Enzymol.* **1981**, *2*, 23–175.
2. Schachter, H. *Curr. Opin. Struct. Biol.* **1991**, *1*, 755–765.
3. Kleene, R.; Berger, E. G. *Biochim. Biophys. Acta* **1993**, *1154*, 283–325.
4. Montreuil, J.; Vliegenthart, J. F. G.; Schachter, H. In *Glycoproteins*; Neuberger, A., van Deenen, L. L. M., Eds.; Elsevier: Amsterdam, 1995; Vol. 29a.
5. Zapun, A.; Petrescu, S. M.; Rudd, P. M.; Dwek, R. A.; Thomas, D. Y.; Bergeron, J. J. M. *Cell* **1997**, *88*, 29–38.
6. Rudd, P. M.; Wormald, M. R.; Stanfield, R. L.; Huang, M.; Mattsson, N.; Speir, J. A.; DiGennaro, J. A.; Fetrow, J. S.; Dwek, R. A.; Wilson, I. A. *J. Mol. Biol.* **1999**, *293*, 351–366.
7. Weis, W. I.; Taylor, M. E.; Drickamer, K. *Immunol. Rev.* **1998**, *163*, 19–34.
8. Marquardt, T.; Freeze, H. *Biol. Chem.* **2001**, *382*, 161–177.
9. Compain, P.; Martin, O. R. *Bioorg. Med. Chem.* **2001**, *9*, 3077–3092.
10. Compain, P.; Martin, O. R. *Curr. Med. Chem.* **2003**, *3*, 541–560.
11. Look, G. C.; Fotsch, C. H.; Wong, C.-H. *Acc. Chem. Res.* **1993**, *26*, 182–190.
12. Sears, P.; Wong, C. H. *Proc. Natl. Acad. Sci. U.S.A.* **1996**, *93*, 12086–12093.
13. Wang, R.; Steensma, D. H.; Takaoka, Y.; Yun, J. W.; Kajimoto, T.; Wong, C.-H. *Bioorg. Med. Chem.* **1997**, *5*, 661–672.
14. Sears, P.; Wong, C. H. *Angew. Chem., Int. Ed.* **1999**, *38*, 2300–2324.
15. Elhalabi, J. M.; Rice, K. G. *Curr. Med. Chem.* **1999**, *6*, 93–116.
16. Waldscheck, B.; Strieff, M.; Notz, W.; Kinzy, W.; Schmidt, R. R. *Angew. Chem., Int. Ed.* **2001**, *40*, 4007–4011.
17. Pauling, L. *Am. Sci.* **1948**, *36*, 51–58.
18. Wolfenden, R. *Nature* **1969**, *223*, 704–705.
19. Schramm, V. L. *Annu. Rev. Biochem.* **1998**, 693–720.
20. Tvaroška, I.; André, I.; Carver, J. P. *J. Am. Chem. Soc.* **2000**, *122*, 8762–8776.
21. Tvaroška, I.; André, I.; Carver, J. P. *Glycobiology* **2003**, *13*, 559–566.
22. Unligil, U. M.; Zhou, S.; Yuwaraj, S.; Sarkar, M.; Schachter, H.; Rini, J. M. *EMBO J.* **2000**, *19*, 5269–5280.
23. Tvaroška, I.; André, I.; Carver, J. P. *J. Phys. Chem. B* **1999**, *103*, 2560–2569.
24. André, I.; Tvaroška, I.; Carver, J. P. *J. Phys. Chem. B* **2000**, *104*, 4609–4617.
25. Compostella, F.; Albini, F. M.; Ronchetti, F.; Toma, L. *Carbohydr. Res.* **2004**, *339*, 1323–1330.
26. Tvaroška, I.; Carver, J. P. *J. Phys. Chem.* **1996**, *100*, 11305–11313.
27. Tvaroška, I.; Bleha, T. *Adv. Carbohydr. Chem. Biochem.* **1989**, *47*, 45–123.
28. Jaguar 5.5, Release 11, Schrödinger, Inc., Portland, OR, 2004.
29. Parallel Quantum Solutions, 2013 Green Acres, Suite A, Fayetteville, AR, 72703.
30. Becke, A. D. *J. Chem. Phys.* **1993**, *98*, 5648–5652.
31. Cramer, C. J. *Essentials of Computational Chemistry. Theories and Models*; Wiley: Chichester, UK, 2002.
32. Tannor, D. J.; Marten, B.; Murphy, R.; Friesner, R. A.; Sitkoff, D.; Nicholls, A.; Ringnalda, M.; Goddard, W. A., III; Honig, B. *J. Am. Chem. Soc.* **1994**, *116*, 11875–11882.